Flat field spectrograph using convex holographic diffraction grating and concave mirror

N C DAS and M V R K MURTY*

Spectroscopy Division, Bhabha Atomic Research Centre, Bombay 400 085, India
*Halo Technologies, Inc., 1008 Brioso Drive, Costa Mesa, California 92627, U.S.A.

Abstract. In this paper we have discussed the aberration properties and the design procedure of a spectrograph which uses a convex holographic grating as the dispersing element and a concave mirror as the focusing element. Both the concave mirror and the convex grating have common axis and they are concentric. The grating is constructed by recording the interference fringes on the convex surface which are formed by two convergent light beams incident from opposite sides of the axis. The illuminating source of the spectrograph is located on a plane perpendicular to the axis and passing through the common centre. It has been found that under certain conditions both positive and negative order spectra are perfectly focused on this plane. Aberration properties of the zero order image as well as the positive and the negative order spectral images have been studied by actual ray tracing. Using this system, design parameters of a medium-sized spectrograph having moderate dispersion and good resolution throughout the UV-visible region of the spectrum have been specified. The performance of the spectrograph has been evaluated by plotting spot diagram.

Keywords. Flat field spectrograph; convex holographic grating; concave mirror; interference fringes; aberration.

PACS No. 7·65; 42·78

I. Introduction

The art of fabricating holographic diffraction grating (Schmahl and Rudolph 1976) is now well established. High quality plane and concave diffraction gratings having straight and equispaced rulings are now being manufactured by holographic method. Also, aberration corrected diffraction gratings having variable spaced curved rulings have been developed by both holographic technique and numerically controlled ruling engine (Harada *et al* 1975, Harada and Kita 1980). Several types of spectrographs and monochromators using simple as well as aberration-corrected holographic diffraction gratings have been designed to cover visible to soft x-ray region of the spectrum. Experimental performances of some of these systems have already been verified. A large number of commercial instruments using holographic diffraction grating are now available from Jobin-Yvon. A simple direct vision spectroscope and an educational type of spectrograph using transmission type of plane holographic diffraction grating have been reported by Murty *et al* 1976 and Shukla *et al* (1983).

Design procedure of holographic grating equipment involves the specifications of

---

the recording geometry and the constructing wavelength for the holographic grating and the geometrical parameters of the instrument, so that aberration-reduced spectral images can be obtained. One of the earlier works in this line is the design of aberration-corrected concave holographic grating for the well-known Seya-Namioka type of monochromator (Seya 1952; Namioka 1954, 1959) which has got excellent focusing properties throughout the vuv to visible region of the spectrum. The possibility of using concave holographic grating in Rowland circle and Seya-Namioka type of mountings has been discussed by Murty and Das (1973), and Namioka et al (1973). It has been concluded that by properly selecting the recording parameters both coma and astigmatism can be reduced by considerable amount. Subsequently, the design procedure of concave holographic grating for Seya-Namioka type of monochromator has been reported by Noda et al. (1974, 1975), and Takahashi and Katayama (1978). Experimental performance of this system has been verified by Namioka et al (1974). It has been established that aberration-corrected holographic grating gives superior performance compared to the conventional mechanically ruled grating and overall performance of the coma-corrected holographic grating is better than that of the astigmatism-corrected concave holographic grating. Subsequently, Pouey (1974) and Lepère (1975) reported the design of stigmatic monochromators for uv region using concave and toroidal holographic diffraction gratings respectively in which the spectrum is scanned by simple rotation of the grating as·in Seya-Namioka type of monochromator.

One of the primary requirements of spectroscopic equipments which record spectral lines on conventional photographic plate or modern diode array detectors is that the images for various wavelengths should be formed on a flat surface with little amount of astigmatism so that all lines can be focused sharply. The fact that by properly selecting the recording and the instrument geometry, imaging characteristics of holographic diffraction gratings can be modified, has led to the design and development of several flat field spectrographs (Pavlycheva 1979; Nilsson 1982, Bittner 1983) using holographic diffraction grating. Very compact systems developed by Nilsson (1982) and Bittner (1983) use concave holographic grating and diode array detector and they can record the entire visible region of the spectrum simultaneously with moderate resolution.

Based on the idea of aplanatic type of diffraction grating by Murty (1960), Murty and Das (1971, 1973) have discussed the construction principle and the aberration properties of both plane and concave holographic gratings having variable spacing circular grooves. It has been established that these gratings can produce aberration-free images corresponding to three wavelengths for both on-axis and off-axis type of illumination. These aberration-free wavelengths are related to the construction wavelength of the holographic grating by simple equations. In the off-axis condition of illumination tangential images for various wavelengths are focused on a zig-zag curve. It has been further suggested by Murty (1976) that high quality spectrum can be recorded if the photographic film is made to conform to the tangential focal curve. Such gratings are now being manufactured by Jobin Yvon. Using concave holographic gratings having variable-spaced circular grooves, Murty and Das (1979, 1980, 1981, 1982) have designed several compact and high aperture monochromators and narrow-band filters in which the grating is used in the on-axis configuration, so that the spectral images do not suffer from astigmatism and coma. These systems, however, use extra optical elements such as, plane mirror, concave mirror, additional concave holographic

grating, etc. The resolution of all these systems near the construction wavelength of the holographic grating is very high and they can be used for scanning the uv-visible region of the spectrum.

For work in the EUV and soft x-ray region of the spectrum, all instruments use grazing incidence mount of the diffracting grating for increasing the reflectivity. In the conventional grazing incidence spectrograph, a concave grating is used in the Rowland circle and the spectrum is recorded on electronic detectors or photographic films which matches the Rowland cylinder. In this system focal lengths vary quite a lot with increasing wavelengths and it suffers from a large amount of astigmatism due to large incident and diffraction angles. In order to minimize these defects, several instruments using toroidal, cylindrical and plane holographic diffraction gratings have been designed and fabricated. For instance, Speer and coworkers (Speer 1974; Speer *et al* 1974) have developed a grazing incidence spectrograph using a toroidal holographic grating with equispaced straight rulings in the Rowland circle mount for recording stigmatic images in the soft x-ray region. Using two interchangeable aberration-corrected toroidal holographic gratings, Fonck *et al* (1982) developed a flat field grazing incidence spectrometer to cover EUV region of the spectrum. A flat-field x-ray spectrograph consisting of a toroidal mirror and a toroidal holographic grating having variable spacing curved grooves has been designed by Chrisp (1983). Along with these grazing incidence spectrographs in which the grating is illuminated by divergent light, some systems where cylindrical and plane holographic gratings are illuminated by convergent light have also been reported. Singh and Singh (1981) discussed the imaging properties of a transmission type of cylindrical holographic grating having variable-spaced curved grooves to be used in the EUV region. Several schemes of grazing incidence spectrograph using both mechanically ruled and holographic plane gratings having variable spaced straight or curved rulings have been reported by Hettrick and Bower (1983) very recently. Aberration properties of these systems have been discussed by Hettrick (1984). Using mechanically-ruled concave grating (Harada and Kita 1980) having variable-spaced straight rulings, a flat field grazing incidence spectrograph has also been designed and the experimental performance of this system in the soft-x-ray and EUV region has been published by Kita *et al* (1983) and Edelstein *et al* (1984).

In this paper we report the design procedure and the aberration properties of a flat-field spectrograph which uses the geometry of two-mirror unit magnification system as discussed below. In order to obtain the suitable recording parameters of the holographic grating, first of all we have optimized the unit magnification system.

2. Unit magnification system

The imaging properties of the unit-magnification system as proposed by Offner (1975) and discussed by Kingslake (1978) are shown in figure 1. It consists of a concave mirror M_1 and a convex mirror M_2 having common axis AA' and common centre C. The stop is located at the convex mirror M_2 and the radius of the convex mirror is equal to half the radius of the concave mirror M_1. The object point S and the image point S' which are situated at equal distances from the axis are located on a plane which is perpendicular to the axis and passes through the common centre of curvature C. The system has zero Petzval curvature and is free from chromatic aberration since it consists of reflecting surfaces only. Because of symmetry, coma and distortion are also absent
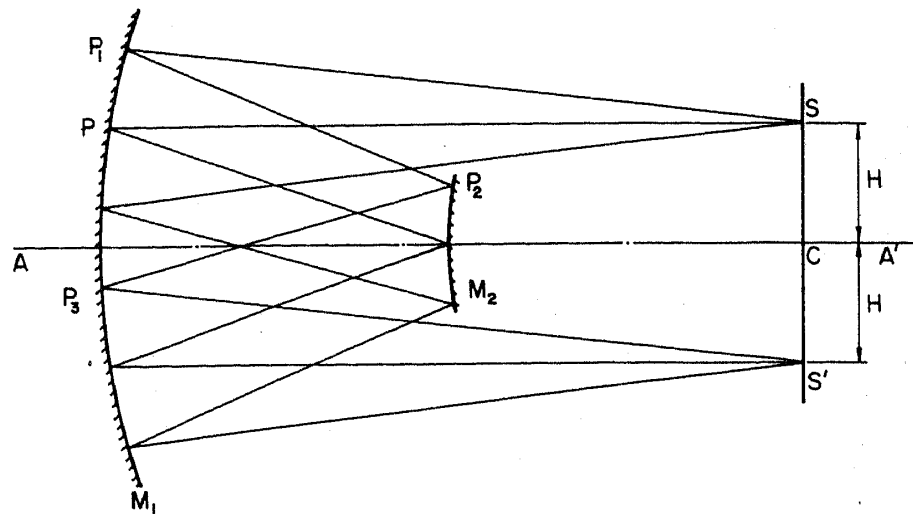
Figure 1. Unit magnification concentric system consisting of concave and convex mirrors.

and the image suffers from higher order spherical aberration and field curvature due to astigmatism.

Detailed analysis of the aberration properties and the optimization procedure of the unit magnification system has been reported by Suzuki (1983). The system has been optimized by small changes of the radius of curvature of the convex mirror and the distance between the two mirrors. The optimized system thus obtained is slightly nonconcentric in which the radius of the convex mirror is exactly equal to half the radius of the concave mirror and the distance between the two mirrors is slightly less than half the radius of the concave mirror. The object plane is, however, slightly away from the centre of curvature of the concave mirror. It has been further suggested that if the concentricity of the system is to be maintained, the optimization of the imagery can be carried out by changing the object height from the axis. For our present study we have followed this procedure and numerical computation of aberrations of the system has been carried out by actual ray tracing. The ray tracing procedure for this unit magnification system has been discussed in Appendix A.

3. Aberration properties of unit magnification system

Detailed analysis by Suzuki (1983) has shown that for the unit magnification concentric system sagittal imagery has no aberration and meridonial imagery suffers from higher order field curvature and residual spherical aberration only. Referring to figure 1, we have therefore computed the focal shift from the ideal image plane SS' and the image blur around the ideal focus S' due to tangential rays only. For this purpose we have traced several meridonial rays originating from the object point S, following the ray tracing scheme of Appendix A. The radius R of the concave mirror M_1 is assumed to be unity and the co-ordinates of the object point S are supposed to be (H, O, R) with respect to the origin located at the pole of the concave mirror M_1.

In order to compute the tangential focal shift two meridonial rays very close to the principal ray SP have been traced. Let us suppose that (k_1', l_1', m_1') and (k_2', l_2', m_2') be the direction cosines of the final reflected rays which meet the ideal image plane SS' at

distances H'_1 and H'_2 from the axis. Then the tangential focal distance H' from the axis and the focal shift Z'_T from the ideal image plane SS' are given by

$$Z'_T = (H'_2 - H'_1)/(k'_1/m'_1 - k'_2/m'_2), \tag{1}$$

$$H = (H'_1 + (k'_1/m'_1)Z'_T. \tag{2}$$

Using (1) and (2) tangential focal shifts and focal distances for images corresponding to several positions of the object point S along the line SS' have been computed and plotted in the form of the curve shown in figure 2.

For computing the blur around the ideal image S', several meridonial rays originating from the object point S and covering the full aperture of the system have been traced and ray aberration curves have been plotted. Ray aberration is simply defined as the deviation of the ray intersection point on the image plane SS' from the ideal image point S'. Typical curves for images corresponding to three object positions described by the object height H are shown in figure 3. In this figure X_1 denotes the aperture variable which is simply the X-coordinate of the ray incident point on the concave mirror M_1 and ε_T is the ray aberration. Referring to figure 1, the permissible f-number of the system for the object height H, so that rays originating from S are not blocked by the convex mirror M_2, is given by

$$f/\# = R/2H. \tag{3}$$

Figure 4 shows the plot of f-number versus the object height H according to (3). For various object positions, image blur has been computed from ray aberration curves and plotted against the f-number. The resulting curve is shown in figure 5.

It may be seen from figure 2 that flat field imagery is possible only when the object points are situated close to the axis of the system and the suitable value for the object distance H is equal to 0·10. From figure 4, one can see that the permissible f-number of the system for that particular object position is $f/5$. Also, from figure 5 it is evident that at this f-number image blur is very small and it practically vanishes beyond $f/7$. Therefore for all practical purposes we may assume that the limiting object height H and the f-number are equal to 0·10 and $f/5$ respectively.

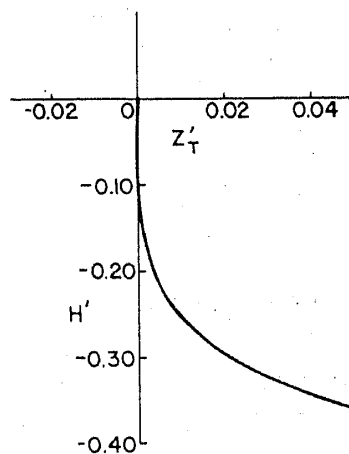In our present analysis we have assumed the radius of the concave mirror to be unity.

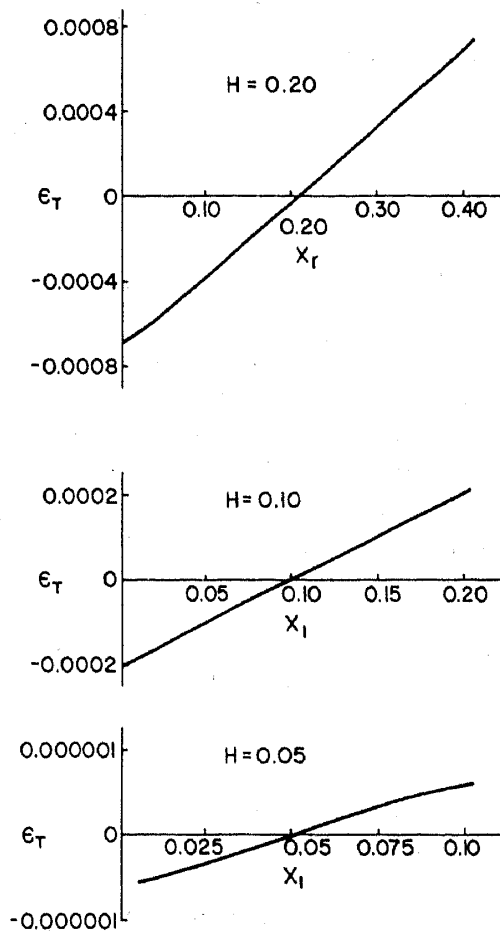**Figure 2.** Tangential focal curve of unit magnification concentric system.

Figure 3. Typical ray aberration curves of unit magnification concentric system for various object positions.
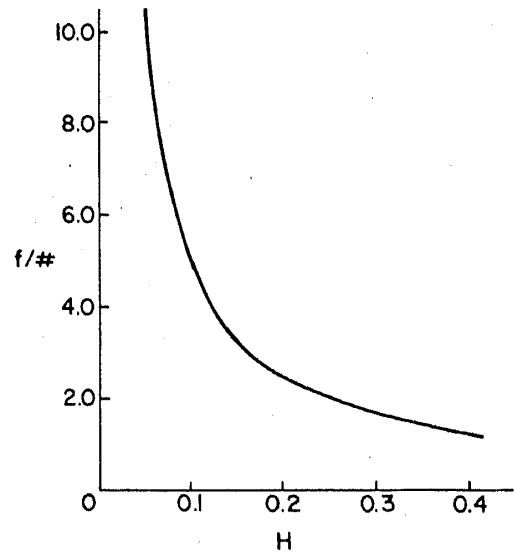
Figure 4. Plot f-number of unit magnification concentric system versus the object height.

For the practical system, however, the exact value of this radius is to be specified. It is well known that for diffraction limited optical system, the physical size of the image blur should not exceed the f-number of the system expressed in micrometer. So the image blur for various f-numbers plotted in figure 5 has been scaled up by an appropriate value for the radius of curvature of the concave mirror to satisfy the above condition of diffraction limited image. Figure 6 shows the plot of the radius of curvature R of the concave mirror against the f-number for diffraction limited imagery. It may be seen that for f-numbers less than $f/5$, the radius of the concave mirror is quite small and consequently the physical size of the system is not reasonable. We, therefore, further conclude that the f-number of the system should be greater than $f/5$.

4. Construction of the holographic grating

In order to discuss the construction principle of the holographic grating for the flat field spectrograph let us refer to figure 1. A convex spherical surface coated with photoresist whose radius is equal to half the radius of the concave mirror M_1 is kept at the position of the convex mirror M_2. It is exposed to two coherent light beams originating from the
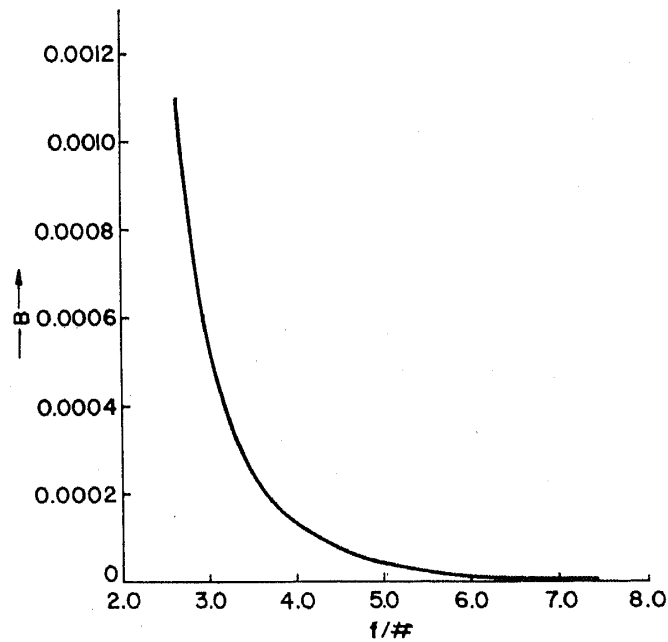
Figure 5. Plot of image blur versus the f-number of the unit magnification concentric system.
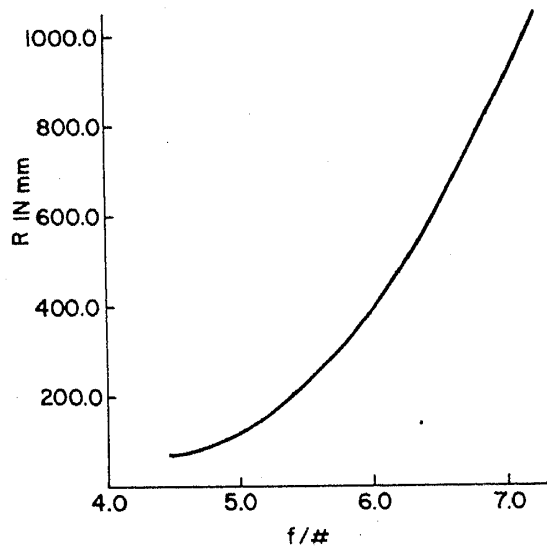

Figure 6. Plot of radius of the concave mirror versus the f-number of the unit magnification concentric system for diffraction limited image.

source points S and S' and reflected by the concave mirror M_1. After exposure and development the spherical surface is coated with reflecting material and is kept at the original recording position of M_2, so that it behaves as a diffraction grating when illuminated by a polychromatic source located at S. Then from holographic principle, an aberration-free image of the constructing wavelength will be formed at S and the zero order image will be formed at the point S'. Aberration properties of this zero order image have already been discussed in the previous section. Positive order images for wavelengths greater than the constructing one will be formed above S whereas negative order spectral images will be formed below S'.

For obtaining the grating spacing at any point P_2 of the holographic grating let us consider the OPD at P_2 which is given by

$$\text{OPD} = (P_2 P_3 + P_3 S') \sim (S P_1 + P_1 P_2). \tag{4}$$

The condition of formation of a groove passing through P_2 is given by

$$\text{OPD} = n\lambda_0, \tag{5}$$

where n is an integer and λ_0 is the construction wavelength of the holographic grating. In order to obtain the expressions for the direction cosines and the length of the ray paths of equation (4) let us assume that the source distance H and the numerical aperture of the constructing beams which is limited by H in accordance with (3), are not very large so that terms higher than third order in the expansion of all the ray tracing equations of Appendix A can be neglected. Based on this assumption the following equations are obtained. In these equations (X_1, Y_1, Z_1), (X_2, Y_2, Z_2) and (X_3, Y_3, Z_3) are the co-ordinates of the points P_1, P_2 and P_3 respectively. As shown in Appendix A, the origin of co-ordinates for P_1 and P_3 is the pole of the mirror M_1 whereas the origin of coordinates for P_2 is the pole of the mirror M_2. For both coordinate systems X-axis is parallel to the line SS' and Y-axis is perpendicular to the plane of the paper whereas the Z-axis is the optical axis of the system.

(i) Path length SP_1:

$$SP_1/R = 1 - H(2X_1 - H)/2R^2. \tag{6}$$

(ii) Direction cosines of the ray SP_1:

$$k_1 = [1 + H(2X_1 - H)/2R^2] (X_1 - H)/R, \tag{7}$$

$$l_1 = [1 + H(2X_1 - H)/2R^2] Y_1/R, \tag{8}$$

$$m_1 = (X_1^2 + Y_1^2)/2R^2 - [1 + H(2X_1 - H)/2R^2]. \tag{9}$$

(iii) Direction cosines of the ray $P_1 P_2$:

$$k_2 = -[1 - H(2X_1 + H)/2R^2] X_1/R, \tag{10}$$

$$l_2 = -[1 - H(2X_1 + H)/2R^2] Y_1/R, \tag{11}$$

$$m_2 = -(X_1^2 + Y_1^2)/2R^2 + [1 - H(2X_1 + H)/2R^2]. \tag{12}$$

(iv) Co-ordinates of the point P_2:

$$X_2/R = [1 + H(2X_1 - H)/2R^2] X_1/2R - [1 + H(2X_1 + H)/2R^2] H/2R, \tag{13}$$

$$Y_2/R = [1 + H(2X_1 - H)/2R^2] Y_1/2R, \tag{14}$$

$$Z_2/R = (X_1^2 + Y_1^2)/4R^2 - H(2X_1 - H)/4R^2. \tag{15}$$

(v) Path length $P_1 P_2$:

$$P_1 P_2/R = 1/2 + H^2/2R^2. \tag{16}$$

(vi) Direction cosines of ray P_2P_3:

$$k_3 = [1 + 3H(2X_1 - 3H)/2R^2]X_1/R - [3 + H(6X_1 - 7H)/2R^2]H/R, \quad (17)$$

$$l_3 = [1 + 3H(2X_1 - 3H)/2R^2]Y_1/R, \quad (18)$$

$$m_3 = (X_1^2 + Y_1^2)/2R^2 - [1 + 3H(2X_1 - 3H)/2R^2]. \quad (19)$$

(vii) Co-ordinates of the point P_3:

$$X_3/R = [1 + 2H(X_1 - H)/R^2]X_1/R - (1 + X_1H/R^2)2H/R, \quad (20)$$

$$Y_3/R = [1 + 2H(X_1 - H)/R^2]Y_1/R, \quad (21)$$

$$Z_3/R = (X_1^2 + Y_1^2)/2R^2 - (X_1 - H)2H/R^2. \quad (22)$$

(viii) Path length P_2P_3:

$$P_2P_3/R = 1/2 + H^2/2R^2. \quad (23)$$

(ix) Direction cosines of the ray P_3S':

$$k' = -[1 + H(2X_1 - H)/2R^2]X_1/R + [1 + H(2X_1 + 3H)/2R^2]H/R, \quad (24)$$

$$l' = -[1 + H(2X_1 - H)/2R^2]Y_1/R, \quad (25)$$

$$m' = -(X_1^2 + Y_1^2)/2R^2 + [1 + H(2X_1 - H)/2R^2]. \quad (26)$$

(x) Path length P_3S':

$$P_3S'/R = 1 + H(2X_1 - 3H)/2R^2. \quad (27)$$

(xi) Co-ordinates of the point S':

$$X' = -H, \quad Y' = 0, \quad Z' = R. \quad (28)$$

Equation (28) shows that when the source point S is situated close to the axis, the zero order image formed at S' is completely free from aberration. Substituting the path lengths from (6), (16), (23) and (27) in (4),

$$\text{OPD} = 2(X_1 - H)H/R. \quad (29)$$

Using (13) and (29) and neglecting terms higher than third order

$$\text{OPD} = 4HX_2/R. \quad (30)$$

Equation (30) shows that when the constructing sources S and S' are close to the axis, OPD at any point P_2 of the recording surface varies linearly with X-coordinate of the point only. Therefore the grooves formed on the recording surface will be straight and parallel to the Y-axis when projected on the X-Y plane.

Using (5) and (30),

$$X_2 = nR\lambda_0/4H. \quad (31)$$

The projected groove spacing in the X-Y plane is simply the derivative of X_2 with respect to the integer n and hence from (31) the groove spacing d_0 is given by

$$\lambda_0/d_0 = 4H/R. \tag{32}$$

Thus we may conclude that when the recording sources are close to the axis, the grating recorded on the convex surface M_2 is equivalent to a mechanically ruled grating having equispaced and straight rulings whose groove spacing is given by (32).

5. Aberrations of unit magnification system in the dispersive mode

Figure 7 shows the imaging principle of the unit magnification system in the dispersive mode where the convex holographic grating G is the dispersing element. When a polychromatic source is located at one of the constructing source position S, the zero order image is formed at the other constructing source position S_0. Positive and negative order images for any wavelength λ are formed at S' and S'_- respectively. Let α be the angle of incidence for the principal ray $P_0 O_2$ and β be the angle of diffraction for the diffracted ray $O_2 P$ for any wavelength λ. Then the equation of diffraction for the wavelength λ is given by

$$\sin \alpha + \sin \beta = \lambda/d_0. \tag{33}$$

It may be seen from (16) that the path length of any reflected ray between the concave mirror M_1 and the grating G is independent of the incident point coordinates based on certain approximations already discussed in the previous section. Hence using (16) for the ray path length $P_0 O_2$, we have from figure 7
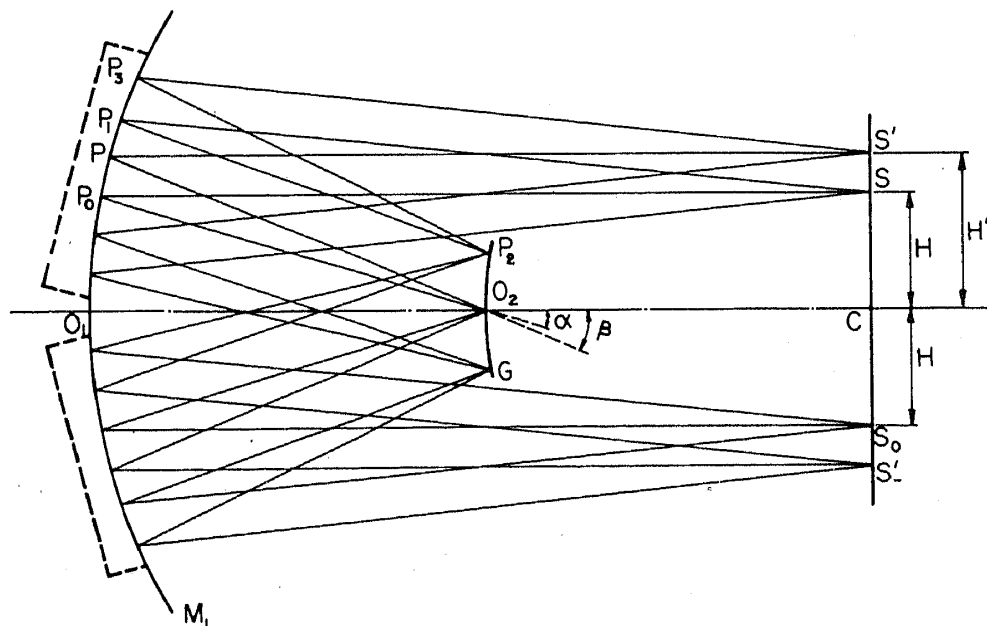
$$\sin \alpha = (H/R)/(1/2 + H^2/2R^2). \tag{34}$$

Figure 7. Layout of spectrograph consisting of concave mirror and convex holographic grating.

The angle of diffraction β is given by

$$\sin \beta = 2H'/R. \tag{35}$$

Using (32) and paraxial approximations of (33) to (35) we have

$$H' = H[2(\lambda/\lambda_0) - 1]. \tag{36}$$

Equation (36) gives the image distance for any wavelength λ from the axis of the system. Reciprocal linear dispersion and the resolution of the system are given by

$$d\lambda/dH' = \lambda_0/2H, \tag{37}$$

$$\Delta\lambda/\lambda_0 = B/2H, \tag{38}$$

where B is the spectral image blur due to tangential rays.

In order to study the aberration properties of the unit magnification system in the dispersive mode, we have assumed that the recording sources are situated close to the axis so that the groove spacing of the holographic grating can be computed by (32). We have also assumed that the radius of the concave mirror to be unity. Referring to figure 7, tangential rays originating from the source point S have been traced following the ray tracing scheme of Appendices A and B. Using the ray trace data, tangential focal shift from the image plane SS_0 and the blur around the paraxial images S' and S'_- for any wavelength λ have been computed following the procedure discussed in §3.

Figures 8 and 9 show the plot of tangential focal shifts at various wavelengths for different positions of the source described by the parameter H. Negative values of wavelengths shown in figure 9 indicate that the spectral images are formed in the negative order. As discussed in §3, the maximum value of H has been taken to be 0·10, which is the limiting distance of the recording sources from the axis, for obtaining diffraction-limited zero-order image on a flat surface. It may be seen from the focal curves that the spectral images are formed almost on a flat surface when the source distance $H = 0·05$. It is evident from (3) that the f-number of the system for this
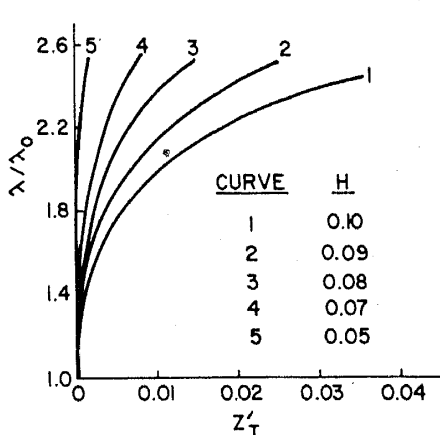

Figure 8. Tangential focal curves for positive order spectral images.
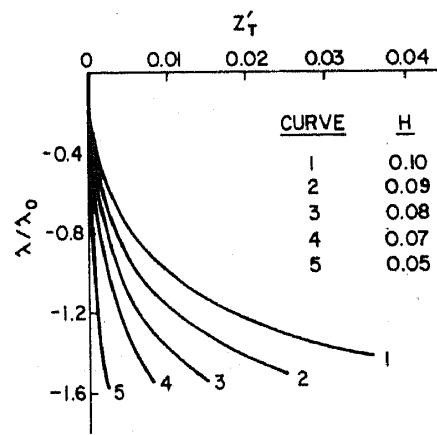
Figure 9. Tangential focal curves for negative order spectral images indicated by negative values of wavelength.
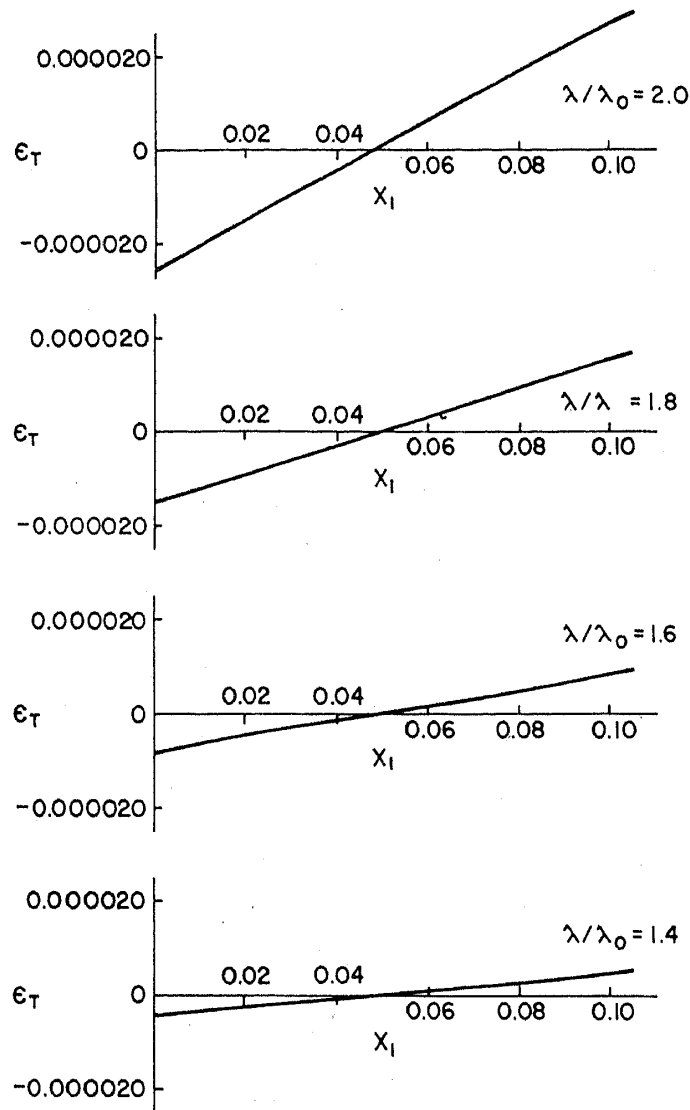
Figure 10. Ray aberration curves for positive order spectral images.

particular source position is $f/10$. So while designing a flat field spectrograph forming aberration-free zero-order image, one may assume that the maximum permissible distance of the recording and reconstructing sources from the axis of the system is equal to 0.05 and the f-number of the system is $f/10$. For this particular source position and f-number, several tangential rays originating from the source have been traced and ray-aberration curves have been plotted. Typical curves are shown in figures 10 and 11. Curves shown in figure 10 are for positive order spectral images whereas curves shown in figure 11 are for negative order spectral images indicated by negative values of the wavelength. From the ray aberration curves we have estimated the blur of spectral images due to tangential rays. Substituting the value of the spectral image blur in (38) resolution of the spectral images at various wavelengths have been computed and plotted against wavelength. The resulting curves for positive and negative order spectral images are shown in figures 12 and 13 respectively. It may be seen that the resolution of the system at wavelengths near the constructing wavelength λ_0 and the
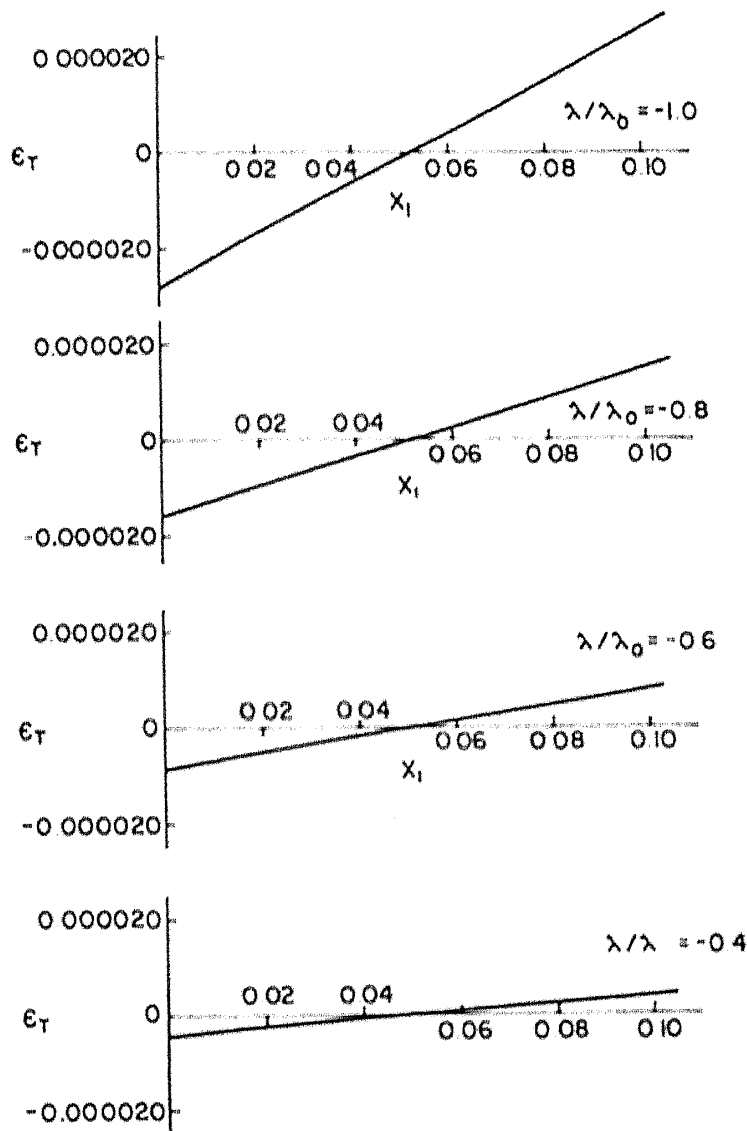
Figure 11. Ray aberration curves for negative order spectral images.

zero order image is very high, since the image blur at these wavelengths is very small. The resolution, however, decreases with increasing wavelength.

6. Flat field spectrograph

While designing a practical holographic grating spectrograph based on the geometry of figure 7, first we are to specify the radii of curvature of the concave mirror M_1 and the holographic grating G, the distance of the source point S from the axis and the constructing wavelength λ_0 for the holographic grating. For flat field imagery we have already concluded in the previous section that the f-number of the system should be $f/10$ and the source distance from the axis should be 0·05 for unit radius of the concave mirror. For a practical system this source distance should be scaled up by the finite radius of the concave mirror. Based on this consideration, we have specified the
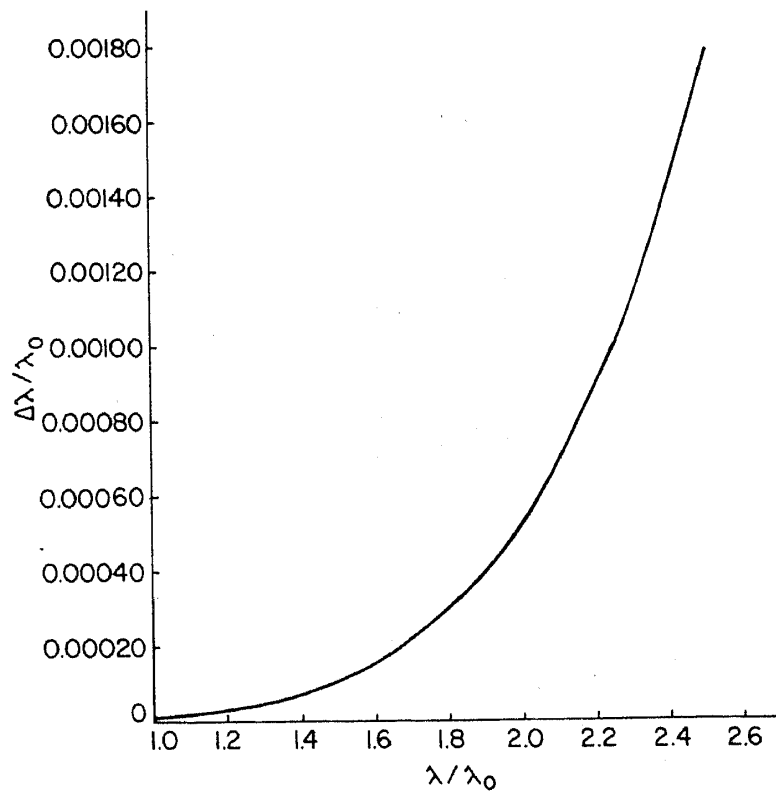
Figure 12. Plot of resolution versus wavelength for positive order spectral images.
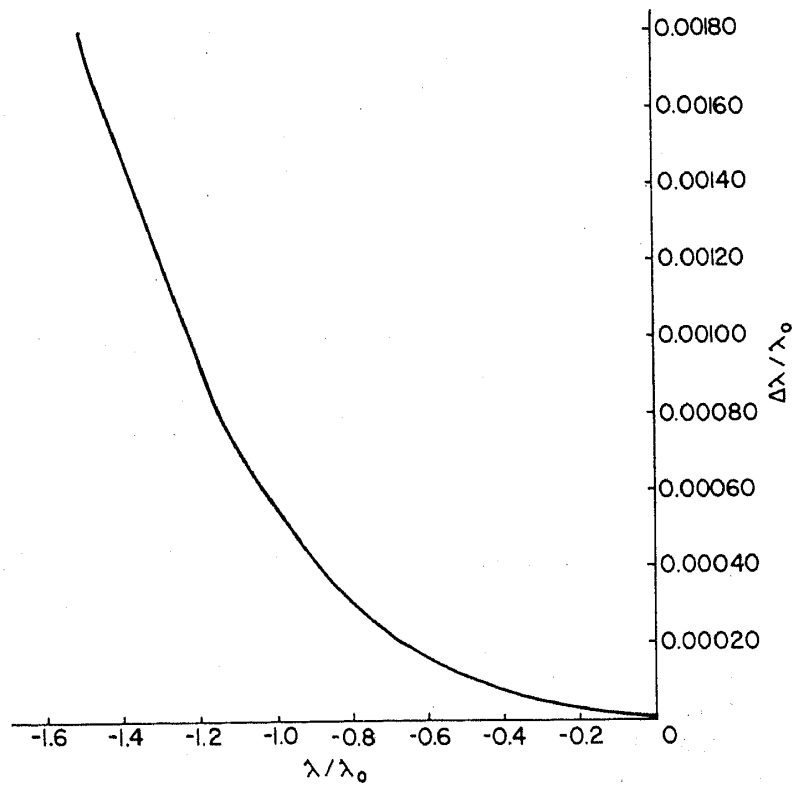

Figure 13. Plot of resolution versus wavelength for negative order spectral images.

following parameter for a medium-sized spectrograph.

Speed of the spectrograph	: $f/10$,
Radius of the concave mirror M_1	: 1000 mm,
Radius of the convex holographic grating G	: 500 mm,
Axial distance between the concave mirror and the grating	: 500 mm,
Distance of the source point S from the axis	: 50 mm.

The construction wavelength λ_0 for the holographic grating has been considered to be 3638 A of argon ion laser or its second harmonic 1819 A. Using (32) and (37), grating frequency and reciprocal linear dispersion of the instrument are obtained as follows.

Grating A:
Construction wavelength	: 3638 Å,
Grating frequency	: 550 lines/mm,
Reciprocal linear dispersion	: 36·4 A/mm.

Grating B:
Construction wavelength	: 1819 Å,
Grating frequency	: 1100 lines/mm,
Reciprocal linear dispersion	: 18·2 A/mm.

Tables 1 and 2 show the theoretical resolution of the spectrograph when it uses gratings A and B respectively as the dispersing elements. The actual values of the wavelength and the theoretical resolution have been obtained by scaling up the wavelength ratio λ/λ_0 and the resolution $\Delta\lambda/\lambda_0$ plotted in figures 12 and 13, by the construction wavelength λ_0. It may be seen from table 1 that while using the low frequency grating A, the spectrograph is suitable for recording visible and uv wavelengths in the positive and the negative order respectively. From table 2 it is evident that using the high frequency grating B, the spectrograph can record uv wavelengths in the positive order. In both cases resolution of the instrument is fairly good.

Table 1. Resolution of the practical spectrograph using low frequency holographic grating constructed by the wavelength 3638 Å. Negative values of wavelength indicate that the images are formed in the negative order.

λ_0 A	λ A	λ/λ_0	$\Delta\lambda/\lambda_0$	$\Delta\lambda$ A
	4000	1·10	0·00002	0·07
	5000	1·37	0·00006	0·22
	6000	1·65	0·00018	0·65
	7000	1·92	0·00043	1·56
	8000	2·20	0·00090	3·27
3638				
	−1000	−0·275	0·00004	0·15
	−2000	0·550	0·00013	0·47
	−3000	−0·825	0·00033	1·20
	−4000	−1·100	0·00070	2·54

Table 2. Resolution of the practical spectrograph using high frequency holographic grating constructed by the wavelength 1819 A. ·

λ_0 A	λ A	λ/λ_0	$\Delta\lambda/\lambda_0$	$\Delta\lambda$ A
	2000	1·10	0·00002	0·04
	2500	1·37	0·00006	0·11
1819	3000	1·65	0·00018	0·33
	3500	1·92	0·00043	0·78
	4000	2·20.	0·00090	1·64

In order to specify the actual size of the grating and the concave mirror, let us refer to figure 7. It may be seen that the incident beam diameter and consequently the *f*-number of the system determine the size of the grating G where the stop is located. Simple geometrical consideration shows that the maximum width of the grating should be slightly less than or equal to the source distance H, so that full cone of the light beam originating from the source point S may be incident on the grating surface without any obstruction. It is to be noted that the diameter of the concave mirror M_1 is determined by the maximum value for the image distance H' corresponding to the upper wavelength of the spectrum to be recorded. If the system is meant for recording both positive and negative order spectrum, the maximum diameter of the concave mirror for focusing the full cone of the diffracted beam of the image point S' is approximately given by

$$\phi = 2(H' + H), \tag{39}$$

where the image distance H' for the extreme wavelength can be computed by (36). It has been found by actual computation that the diameter required for the concave mirror of the present system is very large. So the most practical proposition is to use two identical concave mirrors in the off-axis configuration whose outlines are shown by dotted lines in figure 7 and whose radius is equal to the radius of the concave surface M_1. For recording the positive order spectrum only the upper mirror is to be used. Both the upper and the lower mirrors, however, are to be used when either the negative or both the negative and the positive order spectra are to be recorded. Based on the above considerations we have specified the size of the grating G and the diameter of each concave mirror required for recording visible and uv wavelengths as follows.

grating size   : 50 × 50 mm,
diameter of each concave mirror   : 220 mm.

It may be further seen from figure 7 that while constructing the holographic grating, full cones of the two coherent light beams originating from the source points S and S_0 will be overlapped on the maximum width of the recording surface G, provided the aperture of the concave surface M_1 is equal to four times the source distance H. Therefore from the already presented data for the diameter of each concave mirror and the source distance H, it is evident that only one of the two concave mirrors may be mounted in the on-axis configuration while constructing the holographic grating.

The flat-field spectrograph whose geometrical parameters are specified above and which uses the low frequency grating *A* as the dispersing element and two off-axis concave mirrors as the focusing elements has been evaluated by plotting the spot diagram. For this purpose the spectrograph is supposed to be illuminated by a line source passing through the point *S* and perpendicular to the meridonial plane. The mid-point of the line source is located at the point *S*. A large number of rays originating from the two extreme points, the mid-point and two intermediate points of the line source and covering the full aperture of the grating, have been traced using the equations of Appendices A and B. Figure 14 shows the spot size at various wavelengths when the length of the illuminating source is 10 mm. The horizontal axis of the spot diagram represents the width of the spectral lines in micrometer and the vertical axis represents the length of the spectral lines in mm. It is to be noted that there is no lengthening of the
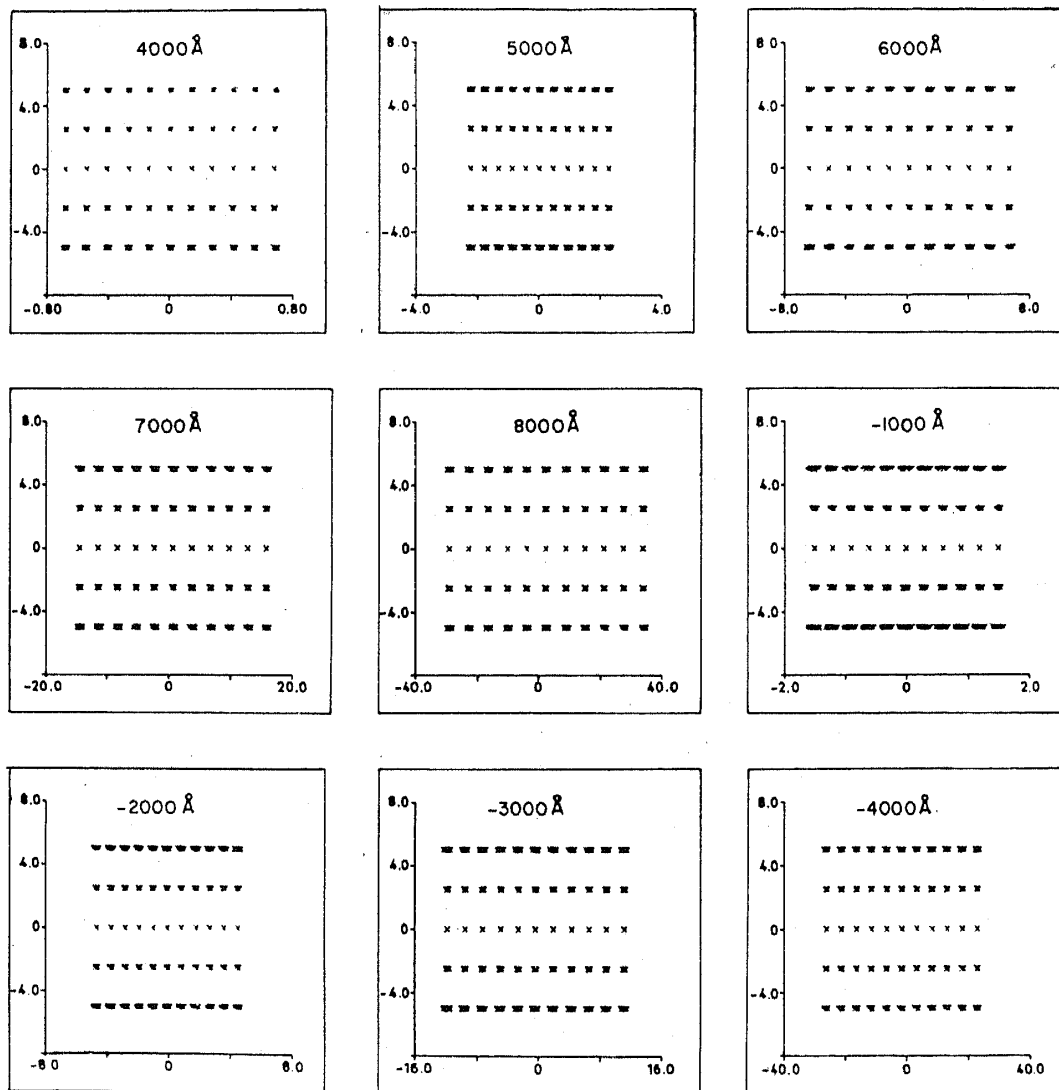

Figure 14. Spot diagram of the practical spectrograph at various wavelengths using a 10-mm line source. Horizontal axis represents spectral image blur in μm and the vertical axis represents the length of the spectral image in mm. Negative values of wavelength indicate negative order spectral images.

spectral lines due to astigmatism and they are broadened symmetrically due to spherical aberration only.

Referring to figure 7, the volume of the spectrograph can be reduced to half if only the upper mirror is used as the focusing element. In this case one can record only the positive order spectrum. Under this situation, gratings A and B should be used in succession for recording visible and uv wavelengths respectively. Thus using two focusing mirrors one can simultaneously record uv and visible wavelengths, whereas using only one focusing mirror one can record only one region of the spectrum depending on the particular grating used. We have considered that the convex grating is to be fabricated by the holographic method. Since it will have straight and equispaced rulings, it may be fabricated by conventional ruling engine also. The use of holographic grating produces stray light and ghost-free images whereas by using mechanically ruled grating energy may be concentrated near a particular wavelength by choosing a proper blaze angle.

Finally we may conclude that a medium size spectrograph having flat field, moderate dispersion and good resolution properties throughout the uv-visible region of the spectrum may be fabricated using the layout and geometrical parameters already discussed.

Acknowledgements

Appendix A: Ray tracing scheme for unit magnification system in the reflective mode

Figure 15 shows the ray paths and coordinate system of the unit magnification system consisting of a concave mirror M_1 and convex mirror M_2 having common centre C. Let us suppose that R is the radius of the concave mirror M_1 and the distance between the concave and the convex mirror is $R/2$. Following Kingslake (1978), and Spencer and
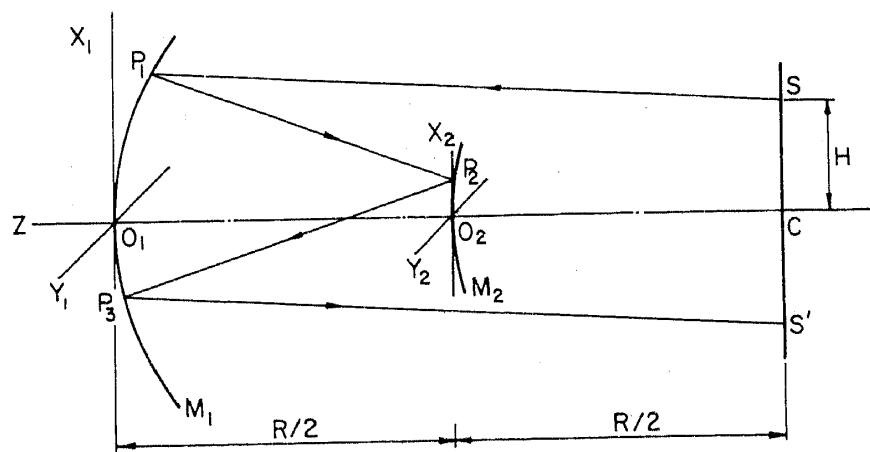

Figure 15. Ray diagram and coordinate system for the unit magnification concentric system.

Murty (1962), we have formulated the direction cosines of the reflected rays $P_1 P_2$, $P_2 P_3$ and $P_3 S'$ and the coordinates of the ray incident points P_1, P_2 and P_3 according to the following scheme.

(H, h, R) – Coordinates of the object point S with respect to the origin located at the pole O_1 of the concave mirror M_1.

(X_1, Y_1, Z_1) – Coordinates of the ray incident point P_1 with respect to the origin at O_1.

(X_2, Y_2, Z_2) – Coordinates of the ray incident point P_2 with respect to the origin located at the pole O_2 of the convex mirror M_2.

(X_3, Y_3, Z_3) – Coordinates of the ray incident point P_3 with respect to the origin O_1.

(X', Y', Z') – Coordinates of the ray intersection point S' with the image plane SS' with respect to the origin at O_1.

Based on the above scheme the following equations are obtained.

(i) Path length of the ray SP_1:

$$SP_1 = [(X_1 - H)^2 + (Y_1 - h)^2 + (Z_1 - R)^2]^{1/2};$$
$$Z_1 = R - [R^2 - (X_1^2 + Y_1^2)]^{1/2}. \tag{40}$$

(ii) Direction cosines of the ray SP_1:

$$k_1 = (X_1 - H)/SP_1; \quad l_1 = (Y_1 - h)/SP_1; \quad m_1 = (Z_1 - R)/SP_1. \tag{41}$$

(iii) Direction cosines of the normal at P_1:

$$K_1 = -X_1/R; \quad L_1 = -Y_1/R; \quad M_1 = 1 - Z_1/R. \tag{42}$$

(iv) Direction cosines of the reflected ray $P_1 P_2$:

$$k_2 = k_1 - 2a_1 K_1; \quad l_2 = l_1 - 2a_1 L_1; \quad m_2 = m_1 - 2a_1 M_1; \tag{43}$$

$$a_1 = (k_1 K_1 + l_1 L_1 + m_1 M_1)/(K_1^2 + L_1^2 + M_1^2). \tag{44}$$

(v) Path length D_{12} of the ray $P_1 P_2$:

$$D_{12} = -B_1 - (B_1^2 - C_1)^{1/2};$$
$$B_1 = k_2 X_1 + l_2 Y_1 + m_2(Z_1 - R); \tag{45}$$
$$C_1 = X_1^2 + Y_1^2 + (Z_1 - 0.5 R)^2 - R(Z_1 - 0.5 R).$$

(vi) Coordinates of the point P_2:

$$X_2 = X_1 + k_2 D_{12}; \quad Y_2 = Y_1 + l_2 D_{12}; \tag{46}$$
$$Z_2 = (Z_1 - 0.5 R) + m_2 D_{12}.$$

(vii) Direction cosines of the normal at P_2:

$$K_2 = -2X_2/R; \quad L_2 = -2Y_2/R; \quad M_2 = 1 - 2Z_2/R. \tag{47}$$

(viii) Direction cosines of the reflected ray $P_2 P_3$:

$$k_3 = k_2 - 2a_2 K_2; \quad l_3 = l_2 - 2a_2 L_2; \quad m_3 = m_2 - 2a_2 M_2. \tag{48}$$

$$a_2 = (k_2K_2 + l_2L_2 + m_2M_2)/(K_2^2 + L_2^2 + M_2^2). \tag{49}$$

(ix) Path length D_{23} of the ray P_2P_3:

$$D_{23} = -B_2 + (B_2^2 - C_2)^{1/2}; \quad B_2 = k_3X_2 + l_3Y_2 + m_3(Z_2 - 0.5R); \tag{50}$$

$$C_2 = X_2^2 + Y_2^2 + (Z_2 + 0.5R)^2 - 2R(Z_2 + 0.5R).$$

(x) Coordinates of the point P_3;

$$X_3 = X_2 + k_3D_{23}; \quad Y_3 = Y_2 + l_3D_{23}; \quad Z_3 = (Z_2 + 0.5R) + m_3D_{23}. \tag{51}$$

(xi) Direction cosines of the normal at P_3:

$$K_3 = -X_3/R; \quad L_3 = -Y_3/R; \quad M_3 = 1 - Z_3/R. \tag{52}$$

(xii) Direction cosines of the reflected ray P_3S':

$$k' = k_3 - 2a_3K_3; \quad l' = l_3 - 2a_3L_3; \quad m' = m_3 - 2a_3M_3. \tag{53}$$

$$a_3 = (k_3K_3 + l_3L_3 + m_3M_3)/(K_3^2 + L_3^2 + M_3^2). \tag{54}$$

(xiii) Path length P_3S':

$$P_3S' = (R - Z_3)/m'. \tag{55}$$

(xiv) Coordinates of the point S':

$$X' = X_3 + (R - Z_3)k'/m'; \quad Y' = Y_3 + (R - Z_3)l'/m'; \quad Z' = R. \tag{56}$$

Appendix B: Ray tracing scheme for unit magnification system in the dispersive mode

In this case we follow the same ray diagram as shown in figure 15 keeping in mind that the spherical surface M_2 represents a convex reflection grating and P_2P_3 is the diffracted ray for any wavelength λ. For tracing a ray originating from the source point S one can use the equations of Appendix A, except that the direction cosines of the diffracted ray P_2P_3 are given by the following equations which have been specified following Spencer and Murty (1962).

$$k_3 = k_2 - \Lambda u_2 + \Gamma_f K_2; \quad l_3 = l_2 - \Lambda v_2 + \Gamma_f L_2; \quad m_3 = m_2 - \Lambda w_2 + \Gamma_f M_2. \tag{57}$$

The significance of u_2, v_2, w_2 and Γ_f have been discussed by Spencer and Murty (1962). For the convex grating we have

$$u_2 = -1/[1 + K_2^2/(L_2^2 + M_2^2)]^{1/2}; \quad v_2 = -K_2L_2u_2/(L_2^2 + M_2^2). \tag{58}$$

$$w_2 = -K_2M_2u_2/(L_2^2 + M_2^2); \quad \Lambda = \lambda/d. \tag{59}$$

In (59) d represents the local grating spacing at any point P_2 of the grating which is related to the projected grating spacing d_0 in the X-Y plane by the simple equation

$$d = d_0/|u_2|. \tag{60}$$

For the holographic grating the projected grating spacing d_0 can be obtained from (32). The multiplier Γ_f in (57) can be determined from the following iteration formula

$$\Gamma_{n+1} = (\Gamma_n^2 - b_2')/2(\Gamma_n + a_2), \qquad (61)$$

where b_2' is given by

$$b_2' = [\Lambda^2 - 2\Lambda(k_2 u_2 + l_2 v_2 + m_2 w_2)]/(K_2^2 + L_2^2 + M_2^2). \qquad (62)$$

In order to use the iteration equation (61), the first approximation of Γ may be assumed to be

$$\Gamma_1 = b_2'/2a_2 - 2a_2. \qquad (63)$$

References

Bittner R 1983 *Optik* **64** 185

Chrisp M P 1983 *Appl. Opt.* **22** 1519

Edelstein J, Hettrick M C, Mrowka S, Jelinsky P and Martin C 1984 *Appl. Opt.* **23** 3267

Fonck R J, Ramsey A T and Yelle R V 1982 *Appl. Opt.* **21** 2115

Harada T and Kita T 1980 *Appl. Opt.* **19** 3987

Harada T, Moriyama S and Kita T 1975 *Proc. ICO. Conf. Opt. Methods in Sci. and Ind. Meas.*, Tokyo 1974 *J. Appl. Phys. Jpn.* 14, Suppl. 14-1 p.175

Hettrick M C 1984 *Appl. Opt.* **23** 3221

Hettrick M C and Bowyer S 1983 *Appl. Opt.* **22** 3921

Jobin-Yvon *Handbook of Diffraction Grating—Ruled and Holographic*, Jobin-Yvon Optical systems, Division of Jobin-Yvon Diffraction Grating Inc. pp. 28

Kingslake R 1978 *Lens design fundamentals* (New York, San Francisco, London: Academic Press) pp. 321, 145, 298

Kita T, Harada T, Nakano N and Kuroda H 1983 *Appl. Opt.* **22** 512

Lepère D 1975 *Nouv. Rev. Opt.* **6** 173

Murty M V R K 1960 *J. Opt. Soc. Am.* **50** 923

Murty M V R K 1976 *Indian J. Phys.* **50** 162

Murty M V R K and Das N C 1971 *J. Opt. Soc. Am.* **61** 1001

Murty M V R K and Das N C 1973 *J. Opt. (India)* **2** 53, 63

Murty M V R K and Das N C 1979 *J. Opt. (India)* **8** 94

Murty M V R K and Das N C 1980 *J. Opt. (India)* **9** 27

Murty M V R K and Das N C 1981 *J. Opt. (India)* **10** 25, 68

Murty M V R K and Das N C 1982 *J. Opt. Soc. Am.* **72** 1714

Murty M V R K, Narasimham A L and Shukla R P 1976 *Indian J. Pure Appl. Phys.* **14** 406

Namioka T 1954 *Sci. Light (Tokyo)* **3** 15

Namioka T 1959 *J. Opt. Soc. Am.* **49** 951

Namioka T, Noda H and Seya M 1973 *Sci. Light* (Tokyo) **22** 77

Namioka T, Noda H and Seya M 1974 *J. Spectrosc. Soc. Jpn* 23 Suppl. 1, p. 29

Nilsson L E 1982 Research in optics (Annual Report Institute of Optical Research, Sweden) p. 16

Noda H, Namioka T and Seya M 1974 *J. Opt. Soc. Am.* **64** 1043

Noda H, Namioka T and Seya M 1975 *Proc. ICO. Conf. Opt. Methods Sci. and Ind. Meas.* Tokyo (1974 *J. Appl. Phys. Jpn.* 14, Suppl. 1, p. 187)

Offner A 1975 *Opt. Eng.* **14** 130

Pavlycheva N K 1979 *Sov. J. Opt. Technol.* **46** 394

Pouey M 1974 *Appl. Opt.* **13** 2739

Schmahl G and Rudolph D 1976 *Progress in optics* (ed.) E Wolf (Amsterdam, New York, Oxford: North Holland) Vol. 14, p. 197

Seya M 1952 *Sci. Light (Tokyo)* **2** 8

Shukla R P, Das N C and Murty M V R K 1983 *J. Opt. (India)* **12** 107

Singh M and Singh S 1981 *Appl. Opt.* **20** 153
Speer R J 1974 *J. Spectrosc. Soc. Jpn.* **23** Suppl. 1, p. 53
Speer R J, Turner D, Johnson R L and Rudolph D and Schmahl G 1974 *Appl. Opt.* **13** 1258
Spencer G H and Murty M V R K 1962 *J. Opt. Soc. Am.* **52** 672
Suzuki A 1983 *Appl. Opt.* **22** 3943, 3950
Takahashi A and Katayama T 1978 *J. Opt. Soc. Am.* **68** 1254